Journal of Colloid and Interface Science **232,** 86–101 (2000)
doi:10.1006/jcis.2000.7194, available online at http://www.idealibrary.com on IDEAL®

# Depletion Interactions Produced by Nonadsorbing Charged and Uncharged Spheroids

Martin Piech and John Y. Walz[1]

*Department of Chemical Engineering, Yale University, P.O. Box 208286, New Haven, Connecticut 06520*

Received April 24, 2000; accepted August 30, 2000

**The effect of macromolecule shape on the depletion attraction between two hard spherical particles in a solution with nonadsorbing hard spheroidal macromolecules of arbitrary size and aspect ratio was investigated using a modified form of the force-balance model of J. Y. Walz and A. Sharma (1994,** *J. Colloid Interface Sci.* **168, 495). The macromolecules were represented as general spheroids, which could be either charged or uncharged. For the uncharged case, a set of analytical expressions describing the depletion attraction, valid for particles much larger than the characteristic macromolecule size, was developed. Comparisons with the case of spherical macromolecules were made under the condition of either constant macromolecule number density, $\rho_b$, or constant volume fraction, $\phi$. It was found that increasing the spheroidal macromolecule aspect ratio (major axis length/minor axis length) decreases the depletion attraction at constant $\rho_b$, but increases the interaction at constant $\phi$. In the latter case, the interaction produced by prolate macromolecules is greater than that produced by oblate macromolecules of equal axis lengths, while the opposite is true at constant $\rho_b$. A simple scaling analysis is used to explain these trends. Surface charge is found to increase both the range and the magnitude of the depletion attraction; however, the general trends are the same as those found in the uncharged systems. Finally, the effect of the depletion attraction produced by spherical and spheroidal macromolecules on the stability of a dispersion of charged particles was examined. It was found that charged spheroids at concentrations of order 1% volume can produce secondary energy wells of sufficient magnitude to induce flocculation in a dispersion of charged spherical particles.**



*Key Words:* **colloidal forces; depletion forces; depletion interaction; depletion attraction; nonspherical particles.**

## INTRODUCTION

The depletion interaction, which arises between colloidal particles in the presence of a nonadsorbing material (depletant), has been the subject of much research over the past 50 years. A primary reason for this research is the widespread importance of the interaction in various colloidal processes. For example, depletion forces have been found to alter the stability of colloidal suspensions (1–21), to control phase transitions in colloid–polymer and colloid–colloid mixtures (22–29), and to modify the bending modulus of membranes and bilayers (30–32).

The depletion interaction was first satisfactorily explained by Asakura and Oosawa in the mid-1950s (33, 34). These authors showed that a volume exclusion mechanism could lead to a net attraction between two hard, parallel plates in solution with rigid macromolecules. More recent work has shown that the depletion attraction is actually the short-range component of a more general structural interaction (35–40). In one sense, the depletion effect can thus be viewed as a first-order approximation to the structural interaction. When higher order effects are considered (i.e., interactions between the nonadsorbing material), long-range repulsions and even oscillations have been both predicted and observed (32, 36, 39–43, 45). This repulsion is thought to be the primary cause of the so-called depletion stabilization effect observed at higher depletant concentrations (3–5, 16–20).

Although Asakura and Oosawa later extended their original work to the cases of charged and nonspherical depletants (i.e., spheroidal, rod-like, and flexible chain macromolecules were considered), the majority of modeling work completed to-date has focused on systems of hard, uncharged spherical macromolecules. Only very recently have rod-like macromolecules been considered in the context of depletion interactions, even though such macromolecules are present in a large variety of natural and synthetic systems (22, 46–48). For example, Mao *et al.* investigated the depletion interaction between large spheres (radius $R$) caused by mutually avoiding thin hard rods of length $L$, diameter $D$, and bulk number density $\rho_b$ (45). The osmotic pressure exerted on a hard wall by a solution of these rods was calculated from the density of rod ends in contact with the wall (the analog of Henderson's formula for the case of hard spheres (49)). The force between two spherical particles was then found by applying the Derjaguin approximation (50, 51). The magnitude of the attraction at contact between the particles was on the order of $\rho_b kT R L^2$, which is the same scaling as the depletion energy produced by small spheres with diameter equal to the rod length. Furthermore, because the number density of rods can greatly exceed the number density of spheres for the same volume fraction, much larger attractions are possible with rods than with spheres (34, 45, 52). This was confirmed experimentally by Koenderink *et al.* (26), who found evidence for a

[1] To whom correspondence should be addressed.

0021-9797/00 $35.00

depletion-induced fluid–solid transition in a mixture of silica spheres and silica-coated boehmite rods in dimethylformamide solutions at rod concentrations well below the isotropic–nematic transition (volume fractions from 0.33 to 0.50%).

In a later publication, Mao *et al.* (40) solved a self-consistent integral equation describing the density profile of rods between two parallel plates. Again, the Derjaguin approximation was used to extend this result to the interaction of two spherical particles. Their calculations, correct to the third order in rod concentration, indicate that typical colloidal sphere/rod mixtures will exhibit a smaller repulsive barrier than the thermal energy, kT, throughout the semidilute concentration range of the rods. It should be noted, however, that these calculations apply only in the $L/D \gg 1$ limit and are subject to corrections of order $D/L$. Furthermore, use of the Derjaguin approximation restricts applicability of this method to particles that are large compared to the rod length.

Yaman *et al.* (30, 53) developed a model for depletion interactions between spherical particles immersed in a dilute solution of rigid rods without this limitation in rod dimensions (i.e., $L \approx R$ was permitted). The authors found the Derjaguin approximation to be quite accurate as long as $L/R \ll 1$ (i.e., for $L/R \lesssim 0.05$), but large and systematic deviations appear with increasing $L/R$ ratios. For example, for $L/R$ values of 0.2 and 1.0, the deviation was 10 and 50%, respectively.

The model of Yaman *et al.* was based on the calculation of the excess surface energy for two surfaces in contact with a rod solution. The depletion force was calculated from the derivative of the free energy with respect to the separation distance between these two interacting surfaces. Because rod–rod interactions were ignored, this model is correct only to first order in rod concentration and predicts no long-range repulsion. The excess surface energy can also be calculated with the model of Groh *et al.* (32), correct to second order in rod concentration. Because steric interactions between rods are taken into account, the results from the Groh *et al.* model are applicable to more concentrated solutions (i.e., the semidilute regime below the isotropicnematic transition). It should be noted that although the models mentioned above apply to infinitely thin rods, they may nonetheless be fairly accurate even for aspect ratios ($L/D$) as small as 10 (54).

In this paper, we modify the force balance model of Walz and Sharma (42) to calculate depletion interactions between spherical particles in a solution with spheroidal macromolecules correct to first order in macromolecule concentration. One major advantage of using the general spheroidal shape is that a wide range of macromolecule shapes can be accommodated (i.e., needles, thin disks, spheres, and prolate or oblate spheroids of arbitrary aspect ratio). This facilitates modeling of many real systems, such as polymers in low-salt solutions (rod-like shapes), natural and synthetic clay suspensions (disk-like shapes), and various biological systems (e.g., viruses with different spheroidal shapes). Moreover, because the Derjaguin approximation is not employed, the method is applicable to particles and macromolecules of any size. The primary assumption is that the macromolecule concentration is low enough that second-order concentration effects arising from interactions between the macromolecules themselves can be ignored. In the case of hard, uncharged systems, we compare our numerical results to analytical expressions for the depletion interaction between two large particles in a solution of spheroidal macromolecules for the limiting case when $\alpha$ (the largest dimension of the macromolecules) is much less than $R$ (the particle radius).

We have also extended this model to the case where both the particles and the spheroidal macromolecules possess a net surface charge. Electrostatic interactions between the particle and macromolecule are calculated using the perturbation expansion method of Hsu and Liu (55, 56) for the case of constant potential surfaces. Comparisons between the charged and the uncharged systems containing spheroidal macromolecules are presented.

## THEORY

### *Force Balance on a Colloidal Particle*

The force balance model used here follows the same approach presented by Walz and Sharma (42). The schematic of the system is depicted in Fig. 1, where two spherical particles of radius $R$, separated by gap width $h$, are immersed in an isotropic solution of nonadsorbing spheroidal macromolecules of semimajor and semiminor axis lengths $\alpha$ and $\beta$, respectively, and bulk number density (number/volume), $\rho_b$. For the similar system of *spherical* macromolecules, the total force exerted on particle 1 can be calculated as (42)

$$\mathbf{F}_1(h) = \int_{\mathbf{x}} \rho(\mathbf{x}) \nabla_1 E_1(\mathbf{x})\, d\mathbf{x}, \qquad [1]$$

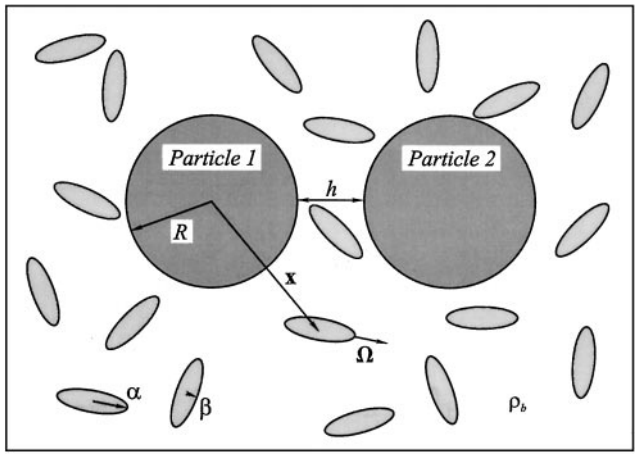


**FIG. 1.** Schematic defining the variables used in the depletion force equations. Two spherical particles of radius $R$ are interacting across gap width $h$ in a solution of spheroidal macromolecules at bulk concentration $\rho_b$. The bulk solution is isotropic, consisting of uniform macromolecules in random orientations $\mathbf{\Omega}$. The vector $\mathbf{x}$ defines the position of a macromolecule relative to the center of particle 1, while parameters $\alpha$ and $\beta$ represent the macromolecule semimajor and semiminor axes, respectively.

where $\rho(\mathbf{x})$ is the number density of macromolecules at position $\mathbf{x}$ and $\nabla_1 E_1(\mathbf{x})$ is the gradient of the interaction energy with respect to the surface of particle 1. This equation is the result of a simple force balance over all macromolecules present in the solution. In the limit of low macromolecule concentrations, the macromolecule distribution around the two particles will follow a Boltzmann distribution of the form

$$\rho(\mathbf{x}) = \rho_b \exp\left[\frac{-E(\mathbf{x})}{kT}\right] \quad [2]$$

where $\rho_b$ is the macromolecule concentration in the bulk, kT is the thermal energy, and $E(\mathbf{x})$ is the potential energy of a macromolecule at position $\mathbf{x}$. When two such particles, 1 and 2, are present (see Fig. 1), the resulting energy can be approximated as the sum of the two individual energies:

$$E(\mathbf{x}) = E_1(\mathbf{x}) + E_2(\mathbf{x}). \quad [3]$$

Substituting Eqs. [2] and [3] into [1] yields

$$\mathbf{F}_1(h) = \int_{\mathbf{x}} \rho_b \exp\left\{-\frac{[E_1(\mathbf{x}) + E_2(\mathbf{x})]}{kT}\right\} \nabla_1 E_1(\mathbf{x})\, d\mathbf{x}. \quad [4]$$

This result can be extended to systems containing spheroidal macromolecules in a straightforward manner. Again, if it is assumed that interactions between macromolecules are not significant (valid for low volume fractions, $\phi$), then the depletion forces produced by macromolecules having different orientations can be added. Now, the integration must be performed over all possible macromolecule positions and orientations. Thus,

$$\mathbf{F}_1(h) = \int_{\mathbf{\Omega}} \int_{\mathbf{x}} \rho_b \exp\left\{-\frac{[E_1(\mathbf{x}, \mathbf{\Omega}) + E_2(\mathbf{x}, \mathbf{\Omega})]}{kT}\right\} \times \nabla_1 E_1(\mathbf{x}, \mathbf{\Omega})\, d\mathbf{x}\, d\mathbf{\Omega}, \quad [5]$$

where the macromolecule orientation is defined by vector $\mathbf{\Omega}$, while $E_1(\mathbf{x}, \mathbf{\Omega})$ and $E_2(\mathbf{x}, \mathbf{\Omega})$ denote the orientation-dependent interaction energies between macromolecules in a given orientation with particles 1 and 2, respectively.

Once the depletion force is known, the interaction energy can be calculated using

$$E_{Dep}(h) = -\int_{\infty}^{h} F_{1,C\text{-}C}(h')\, dh', \quad [6]$$

where $F_{1,C\text{-}C}$ is the component of the force $\mathbf{F}_1$ acting along the line of centers between the two particles. Note that the force balance model was modified in a similar manner by Walz (57) and Piech and Walz (58) to calculate the effect of polydispersity on the depletion interaction in purely spherical systems.

*Forms of the Particle/Macromolecule Interaction*

Before the equations presented above can be evaluated for the depletion force, expressions for the interaction energies between a macromolecule and the two particles, $E_1(\mathbf{x}, \mathbf{\Omega})$ and $E_2(\mathbf{x}, \mathbf{\Omega})$, need to be defined. For the case of simple hard spheres in solution with hard spheroids, these can be written as

$$E_k(\mathbf{x}, \mathbf{\Omega}) = E_{k,HS}(\mathbf{x}, \mathbf{\Omega}) = \begin{cases} +\infty & \text{for particle–macromolecule overlap} \\ 0 & \text{otherwise,} \end{cases} \quad [7]$$

where $k$ is equal to either 1 or 2. Although these expressions are mathematically simple, they can be a poor representation of the interactions in variety of real systems. In aqueous solutions, for example, many surfaces acquire a net electric charge, resulting in long-range electrostatic forces. The expressions for $E_k(\mathbf{x}, \mathbf{\Omega})$ can then be written as

$$E_k(\mathbf{x}, \mathbf{\Omega}) = E_{k,HS}(\mathbf{x}, \mathbf{\Omega}) + E_{k,Elec.}(\mathbf{x}, \mathbf{\Omega}), \quad [8]$$

where $E_{k,Elec.}(\mathbf{x}, \mathbf{\Omega})$ is the electrostatic potential energy of the spheroidal macromolecule and the $k$th spherical particle at position $\mathbf{x}$ and in orientation $\mathbf{\Omega}$.

*Electrostatic Interactions*

An approximate method for predicting the electrostatic free energy of interaction between two charged colloidal particles is the linear superposition approximation (LSA), where it is assumed that two particles are sufficiently spaced such that the total electric potential at any point between them can be approximated as the sum of the potentials produced from each particle. Thus,

$$\psi_{Elec.}(\mathbf{r}, \mathbf{\Omega}) = \psi_{Sphere}(\mathbf{r}) + \psi_{Spheroid}(\mathbf{r}, \mathbf{\Omega}), \quad [9]$$

where $\psi_{Sphere}(\mathbf{r})$ and $\psi_{Spheroid}(\mathbf{r}, \mathbf{\Omega})$ represent the electrostatic potentials at a point $\mathbf{r}$ arising from a spherical particle and a spheroidal macromolecule in orientation $\mathbf{\Omega}$, respectively. The LSA approach has been found to yield accurate results of the interaction energy between two particles for gap widths larger than approximately one Debye length (59). However, since the integration in Eq. [5] is performed over the entire solution volume (therefore all separation distances), using Eq. [9] will result in some error. As discussed in an earlier paper though, this error will tend to be minimal provided that the particles and macromolecules carry a like surface charge and are thus repulsive (58). In this case, $E(\mathbf{x})$ in Eq. [2] or $E_1(\mathbf{x}, \mathbf{\Omega})$ and $E_2(\mathbf{x}, \mathbf{\Omega})$ in Eq. [5] will have large positive values at small gap widths (the region in which LSA slightly overestimates the interaction energy) and the corresponding exponentials in these equations will tend to zero. In other words, the concentration of macromolecules within a few Debye lengths of the particle surface will be small and thus contribute negligibly to the total depletion force.

The expression of Bell *et al.* was used to calculate the electrostatic potential distribution around a spherical particle of radius $R$ and surface potential $\psi_{0,\text{Sphere}}$ in a solution having Debye length equal to $\kappa^{-1}$ (59),

$$y_{\text{Sphere}}(\mathbf{r}) = y_{\text{Sphere}}(r) = 4\tanh\left(\frac{ze\psi_{0,\text{Sphere}}}{\text{kT}}\right)\frac{R}{r}\exp[-\kappa(r-R)], \quad [10]$$

where $y_{\text{Sphere}}(r) = (\frac{ze\psi_{\text{Sphere}}}{\text{kT}})$ is the dimensionless potential at a radial distance $r$ from the center of the particle, $e$ is the proton charge, and $z$ is the valency of the symmetric electrolyte. As stated by Bell *et al.*, this equation is believed to be the correct limiting form of the potential for $\kappa R \geq 10$ and $\psi_{0,\text{Sphere}} \leq 200$ mV (59). If smaller particles are used such that $\kappa R < 10$, alternative expressions for $y_{\text{Sphere}}(\mathbf{r})$ are provided in the Bell *et al.* paper.

The electrical potential distribution around a spheroidal macromolecule can be approximated with the expressions of Hsu and Liu (55, 56), which were derived using a perturbation method to solve the nonlinear Poisson–Boltzmann equation. In this approach, the dimensionless potential at any position in a symmetric electrolyte solution can be written as

$$y_{\text{Spheroid}}(\mathbf{r}, \boldsymbol{\Omega}) = y_{\text{Spheroid}}(\zeta) = \sum_{n=0}^{\infty} \lambda^n Y_n, \quad [11]$$

where $\zeta$ is a function of two spheroidal coordinate variables and represents a dimensionless distance from the spheroid surface, $Y_n$ denotes the $n$th-order perturbation term, and $\lambda$ is the perturbation parameter, defined as the ratio of the Debye length to the length of the spheroid semimajor axis ($\lambda = \kappa^{-1}/\alpha$). Hsu and Liu (55, 56) derived the following analytical expressions for the first two terms in this series

$$Y_0 = 2\ln\left[\frac{1+\eta\exp(-\zeta)}{1-\eta\exp(-\zeta)}\right] \quad [12a]$$

and

$$\begin{aligned} Y_1 = {} & f_1\left[-\text{csch}\left(\frac{Y_0}{2}\right) + \frac{3\ln\eta}{2}\sinh\left(\frac{Y_0}{2}\right)\ln\left(\tanh\left(\frac{Y_0}{4}\right)\right)\right. \\ & \left. - \frac{\ln\eta}{2}\coth\left(\frac{Y_0}{2}\right) - \sinh\left(\frac{Y_0}{2}\right)\ln^2\left(\tanh\left(\frac{Y_0}{4}\right)\right)\right] \\ & - 2f_2\,\text{csch}\left(\frac{Y_0}{2}\right) + \frac{g_1}{2}\left[\coth\left(\frac{Y_0}{2}\right) + \sinh\left(\frac{Y_0}{2}\right)\right. \\ & \left.\times \ln\left(\tanh\left(\frac{Y_0}{4}\right)\right)\right] + g_2\sinh\left(\frac{Y_0}{2}\right), \end{aligned} \quad [12b]$$

where $\eta = \tanh(y_{0,\text{Spheroid}}/4)$, and $y_{0,\text{Spheroid}} = \frac{ze\psi_{0,\text{Spheroid}}}{\text{kT}}$ is the dimensionless surface potential. Explanations of the other terms in the equations above can be found in (56). Higher-order perturbation terms appearing in Eq. [11] can be obtained by numerically solving a set of linear second-order nonhomogenous partial differential equations (56). For the present study, only the first and second terms in the expansion were used.

It should be pointed out that $Y_0$ represents the electrical potential distribution next to a flat plate; thus $Y_1$ can be considered as the first-order correction for curvature effects. This perturbation method is thus most accurate for thin double layers (compared to the macromolecule size) and can be applied to moderate to thick double layers as long as the spheroid aspect ratio (length of semimajor axis/length of semiminor axis) stays sufficiently large. Applicability of this model to the current problem is discussed further under Discussion.

Once the potential distributions around the particle and macromolecule are known, the interaction force between them can be calculated by integrating the total stress tensor over a midpoint plane, perpendicular to a line segment connecting the points of closest approach between the sphere and spheroid. Thus

$$F = \frac{\varepsilon}{2}\left(\frac{\text{kT}}{ze}\right)^2 \int_{\Xi}\left\{2\kappa^2[\cosh y - 1] + \left(\frac{\partial y}{\partial Y}\right)^2 + \left(\frac{\partial y}{\partial Z}\right)^2 - \left(\frac{\partial y}{\partial X}\right)^2\right\} \text{d}\Xi, \quad [13a]$$

where

$$y = y_{\text{Sphere}}(\mathbf{r}) + y_{\text{Spheroid}}(\mathbf{r}, \boldsymbol{\Omega}). \quad [13b]$$

Here $\Xi$ denotes the midpoint plane, $\varepsilon$ is the dielectric permittivity of the solution, and $y$ is the sum of the sphere and spheroid potentials at a point on the $\Xi$ plane. In the $X, Y, Z$, coordinate system referred to here, the $X$ axis lies along the segment connecting the points of closest approach and $\Xi$ is the $Y$–$Z$ plane.

The energy of interaction between the particle and macromolecule for a given macromolecule orientation was found by integrating Eq. [13] from infinite separation to any desired position.

### *Analytical Method for Uncharged Systems*

In this section, analytical expressions for the depletion energy between two hard, uncharged spheres in solution with hard, uncharged, spheroidal macromolecules are presented. This is done by first calculating the change in the surface free energy of a hard flat plate in a solution of hard, nonadsorbing spheroids. This expression is then extended to the case of two parallel plates, separated by gap width $h$. The depletion force between the plates is given by the derivative of this free energy with respect to $h$. Finally, the interaction between two large spheres is found through application of the Derjaguin approximation.

Yaman *et al.* (30) showed that the change in surface free energy (per unit area), $\Delta\gamma$, for any general shape produced by a macromolecule interacting with the surface can be calculated

using

$$\frac{\Delta\gamma}{\rho_b kT} = \int_{\mathbf{x}} S^{-1} \int_{\Omega} \left( \frac{1 - \exp[-U_{ext}(\mathbf{x}, \mathbf{\Omega})]}{4\pi} \right) d\mathbf{\Omega}\, d\mathbf{x}, \quad [14]$$

where the volume integral runs over the space available to the solution, $S$ is the surface area, and $U_{ext}(\mathbf{x}, \mathbf{\Omega})$ is the interaction energy between the surface and a macromolecule at position $\mathbf{x}$ in orientation $\mathbf{\Omega}$. In the case of spheroidal macromolecules between two parallel plates separated by gap $h$ and interacting by hard collisions only, this expression reduces to

$$\frac{\Delta\gamma_{PP}(h)}{\rho_b kT} = \begin{cases} h & \text{for } h < 2\beta \\ 2\int_0^{h/2} \left[1 - \frac{1}{2}\int_\theta \sin\theta\, d\theta\right] dz & \text{for } 2\beta \le h < 2\alpha \\ 2\int_0^{\alpha} \left[1 - \frac{1}{2}\int_\theta \sin\theta\, d\theta\right] dz & \text{for } h \ge 2\alpha, \end{cases} \quad [15]$$

where $\alpha$ and $\beta$ are the spheroid semimajor and semiminor axes, respectively, $z$ is the distance of the macromolecule center from one plate, and $h$ is the gap width. (Because of symmetry, it is necessary to integrate over only half of the gap region.) The inner integration is performed over all allowable configurations characterized by a range of $\theta$ values (see Fig. 2). For prolate spheroids, the integration limits are $\theta_t$ and $(\pi - \theta_t)$, where

$$\theta_t = \sec^{-1}\left(\sqrt{\frac{\alpha^2 - \beta^2}{z^2 - \beta^2}}\right). \quad [16a]$$

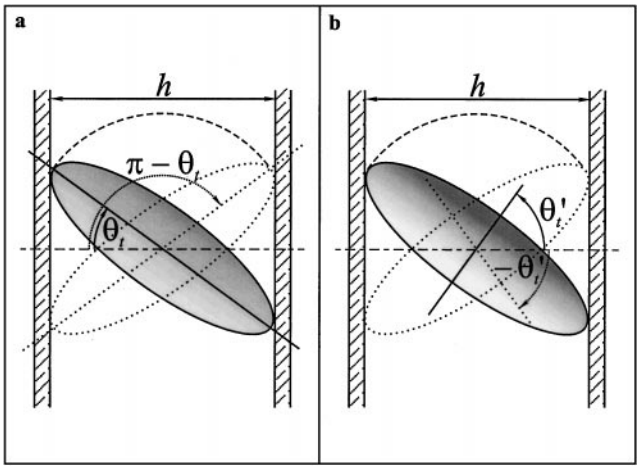


**FIG. 2.** Schematic illustrating the allowable configurations for a spheroid between two hard parallel plates at gap width $h$. (a) Prolate spheroids can access configurations characterized by all angles between $\theta_t$ and $(\pi - \theta_t)$. (b) Orientations accessible to oblate spheroids lie between $\theta_t'$ and $-\theta_t'$. Notice the different definitions of angles $\theta_t$ and $\theta_t'$ in the two cases. In each drawing, the dark line through the spheroid center denotes its axis of revolution.

For oblate spheroids, the integration is carried out from 0 to $\theta_t'$ and from 0 to $-\theta_t'$, where

$$\theta_t' = \frac{\pi}{2} - \sec^{-1}\left(\sqrt{\frac{\alpha^2 - \beta^2}{z^2 - \beta^2}}\right). \quad [16b]$$

Carrying out the integrations in Eq. [15] yields the following expressions for the surface free energy for the cases of prolate and oblate spheroids

$$\frac{\Delta\gamma_{PP,Prolate}(x)}{\rho_b kT\alpha} = \begin{cases} x & \text{for } x < 2A^{-1} \\ x + \frac{1}{A\sqrt{A^2-1}}\left(\ln\left[\frac{Ax + \sqrt{(Ax)^2 - 4}}{2}\right]\right. & \\ \quad \left. - \frac{Ax\sqrt{(Ax)^2-4}}{4}\right) & \text{for } 2A^{-1} \le x < 2 \\ 1 + \frac{\ln[A + \sqrt{A^2-1}]}{A\sqrt{A^2-1}} & \text{for } x \ge 2 \end{cases} \quad [17a]$$

$$\frac{\Delta\gamma_{PP,Oblate}(x)}{\rho_b kT\alpha} = \begin{cases} x & \text{for } x < 2A^{-1} \\ \frac{A}{\sqrt{A^2-1}}\left(\frac{x\sqrt{4-x^2}}{4} - \tan^{-1}\left[\frac{1}{\sqrt{A^2-1}}\right]\right. & \\ \quad \left. + \tan^{-1}\left[\frac{x}{\sqrt{4-x^2}}\right]\right) + A^{-1} & \text{for } 2A^{-1} \le x < 2 \\ \frac{A}{\sqrt{A^2-1}}\left(\frac{\pi}{2} - \tan^{-1}\left[\frac{1}{\sqrt{A^2-1}}\right]\right) + A^{-1} & \text{for } x \ge 2, \end{cases} \quad [17b]$$

where $x = \frac{h}{\alpha}$ is the dimensionless gap width and $A = \frac{\alpha}{\beta}$ is the spheroid aspect ratio.

The depletion force between the plates can be found using

$$\frac{F_{PP}(x)}{S} = -\frac{1}{\alpha}\frac{\partial(\Delta\gamma)}{\partial x}, \quad [18]$$

where $S$ is the plate surface area. Substituting Eqs. [17a] and [17b] into [18] yields the following expressions for the depletion force:

$$\frac{F_{PP,Prolate}(x)}{\rho_b SkT} = \begin{cases} -1 & \text{for } x < 2A^{-1} \\ -1 + \frac{1}{2}\sqrt{\frac{(Ax)^2-4}{A^2-1}} & \text{for } 2A^{-1} \le x < 2 \\ 0 & \text{for } x \ge 2 \end{cases} \quad [19a]$$

$$\frac{F_{PP,Oblate}(x)}{\rho_b SkT} = \begin{cases} -1 & \text{for } x < 2A^{-1} \\ -\frac{A}{2}\sqrt{\frac{4-x^2}{A^2-1}} & \text{for } 2A^{-1} \le x < 2 \\ 0 & \text{for } x \ge 2. \end{cases} \quad [19b]$$

Substituting these expressions into Eq. [6] and integrating yields the following equations for the depletion energy:

$$\frac{E_{\mathrm{PP,Prolate}}(x)}{\rho_b \mathrm{SkT}\alpha} = \begin{cases} x - 1 - \frac{\ln(A+\sqrt{A^2-1})}{A\sqrt{A^2-1}} & \text{for } x < 2A^{-1} \\ x - 1 + \frac{1}{A\sqrt{A^2-1}}\left[\ln\left(\frac{Ax+\sqrt{(Ax)^2-4}}{2(A+\sqrt{A^2-1})}\right) - \frac{Ax\sqrt{(Ax)^2-4}}{4}\right] & \text{for } 2A^{-1} \le x < 2 \\ 0 & \text{for } x \ge 2 \end{cases} \quad [20a]$$

$$\frac{E_{\mathrm{PP,Oblate}}(x)}{\rho_b \mathrm{SkT}\alpha} = \begin{cases} x - \frac{A}{\sqrt{A^2-1}} \times \left[\frac{\pi}{2} - \tan^{-1}\left(\frac{1}{\sqrt{A^2-1}}\right)\right] - A^{-1} & \text{for } x < 2A^{-1} \\ \frac{A}{\sqrt{A^2-1}}\left[\frac{x\sqrt{4-x^2}}{4} + \tan^{-1}\left(\frac{x}{\sqrt{4-x^2}}\right) - \frac{\pi}{2}\right] & \text{for } 2A^{-1} \le x < 2 \\ 0 & \text{for } x \ge 2. \end{cases} \quad [20b]$$

Note that Eq. [20] is essentially the same as Eq. [17], with the only difference being the energy reference state. In Eq. [17], the excess surface free energy is zero at contact between the plates ($x = 0$) and finite positive at infinite separation. On the other hand, the depletion energy given by Eq. [20] is set to zero at infinte gap width and has a negative value at contact. The functional dependence on gap width, however, is exactly the same in both equations.

Finally, applying the Derjaguin approximation (50, 51) to Eq. [20] yields the depletion energy between two spheres in the limit $R \gg \alpha$:

$$\frac{E_{\mathrm{SS,Prolate}}(x)}{\rho_b \pi R\mathrm{kT}\alpha^2} = \begin{cases} x - \frac{x^2}{2} - \frac{2}{3} - \frac{4}{3}A^{-2} + \frac{x}{A\sqrt{A^2-1}}\ln(A+\sqrt{A^2-1}) & \text{for } x < 2A^{-1} \\ x - \frac{x^2}{2} - \frac{2}{3} - \frac{4}{3}A^{-2} + \frac{[(Ax)^2+8]\sqrt{(Ax)^2-4}}{12A^2\sqrt{A^2-1}} + \frac{x}{A\sqrt{A^2-1}}\ln\left(2\frac{A+\sqrt{A^2-1}}{Ax+\sqrt{(Ax)^2-4}}\right) & \text{for } 2A^{-1} \le x < 2 \\ 0 & \text{for } x \ge 2 \end{cases} \quad [21a]$$

$$\frac{E_{\mathrm{SS,Oblate}}(x)}{\rho_b \pi R\mathrm{kT}\alpha^2} = \begin{cases} -\frac{4}{3} - \frac{x^2}{2} + xA^{-1} - \frac{2}{3}A^{-2} + \frac{Ax}{\sqrt{A^2-1}}\left(\frac{\pi}{2} - \tan^{-1}\left[\frac{1}{\sqrt{A^2-1}}\right]\right) & \text{for } x < 2A^{-1} \\ \frac{Ax}{\sqrt{A^2-1}}\left(\frac{\pi}{2} - \tan^{-1}\left[\frac{x}{\sqrt{4-x^2}}\right] - \frac{(x^2+8)\sqrt{4-x^2}}{12x}\right) & \text{for } 2A^{-1} \le x < 2 \\ 0 & \text{for } x \ge 2. \end{cases} \quad [21b]$$

It should be pointed out that expressions for small gap widths ($x < 2A^{-1}$) were published previously by Asakura and Oosawa in a slightly different form (34). However, the equations in the region $2A^{-1} \le x < 2$ are reported here for the first time.

The expressions presented above can be greatly simplified for the limiting cases of rod-like, disk-like, and spherical macromolecules. In the first two cases, $\beta = 0$ and Eqs. [21a] and [21b] reduce to

$$\frac{E_{\mathrm{SS,Needle}}(h)}{\rho_b \pi R\mathrm{kT}L^2} = \begin{cases} \frac{1}{6}\left(\frac{h}{L} - 1\right)^3 & \text{for } h < L \\ 0 & \text{for } h \ge L \end{cases} \quad \text{and } R \gg L \quad [22]$$

and

$$\frac{E_{\mathrm{SS,Disk}}(h)}{\rho_b \pi R\mathrm{kT}D^2} = \begin{cases} \frac{h}{2D}\left(\frac{\pi}{2} - \sin^{-1}\frac{h}{D}\right) - \frac{1}{6}\left(2 + \frac{h^2}{D^2}\right)\sqrt{1 - \frac{h^2}{D^2}} & \text{for } h < D \\ 0 & \text{for } h \ge D \end{cases} \quad \text{and } R \gg D \quad [23]$$

for infinitely thin rods (needles) and disks, respectively. In these equations, $L$ is the rod length and $D$ is the disk diameter. Finally, for spherical macromolecules of radius $a$, $A = 1$ and Eqs. [21a] and [21b] simplify to

$$\frac{E_{\mathrm{SS,Sphere}}(h)}{\rho_b \pi R\mathrm{kT}a^2} = -\begin{cases} 2 - \frac{2h}{a} + \frac{h^2}{2a^2} & \text{for } h < 2a \\ 0 & \text{for } h \ge 2a \end{cases} \quad \text{and } R \gg a, \quad [24]$$

which is an approximation to the more general expression

$$\frac{E_{\mathrm{SS,Sphere}}(h)}{\rho_{\mathrm{b}}\pi\, R\mathrm{k}\mathrm{T}a^2} = -\begin{cases} 2 - \frac{2h}{a} + \frac{h^2}{2a^2} + \frac{4a}{3R} & \\ \quad - \frac{h}{R} + \frac{h^3}{12a^2R} & \text{for } h < 2a \\ 0 & \text{for } h \geq 2a, \end{cases} \quad [25]$$

derived by Asakura and Oosawa (33) for systems containing spherical particles and spherical macromolecules of arbitrary size (i.e., for all $a/R$ values).

## RESULTS

### *Depletion Interactions in Hard Systems—Analytical Model*

The dimensionless depletion force between parallel plates predicted by Eqs. [19a] and [19b] is shown in Fig. 3 for various prolate and oblate spheroidal macromolecules. The macromolecules are modeled as nonadsorbing, hard, and uncharged spheroids that interact with the plates only. With the dimensionless separation distance between the plates defined as $h/\alpha$, the depletion attraction vanishes for $h/\alpha > 2$, i.e., when the gap width is larger than twice the length of the macromolecule semimajor axis. Furthermore, when the spheroid aspect ratio exceeds 10, the results approach those for needles and thin disks calculated with Eqs. [19a] and [19b] in the limit of $\beta = 0$. Figure 4 depicts the dimensionless depletion energy between the plates for prolate and oblate macromolecules (Eqs. [20a] and [20b]). As can be seen, the force and energy produced by oblate spheroids are significantly closer to those for spherical macromolecules than the force and energy produced by prolate spheroids, which is addressed further under Discussion. The spherical macromolecule results shown in the Figs. 3 and 4 are computed from Eqs. [19] and [20] by setting $A = 1$.

The depletion interactions between two 5-$\mu$m-radius spherical particles in solution with various prolate and oblate spheroidal macromolecules are illustrated in Figs. 5 and 6. For this and all subsequent graphs, the depletion energy is scaled by the thermal energy, kT. The particles are treated as hard, uncharged spheres, while the macromolecules are modeled as nonadsorbing, hard, and uncharged spheroids with the semimajor axis length equal to 100 nm. For these cases, we will present the effect of spheroid size at two different conditions. In Fig. 5, for example, the macromolecule number density is held constant as the macromolecule shape (i.e., the spheroid aspect ratio) changes. In this case, the macromolecule volume fraction is allowed to vary and *decreasing* the spheroid aspect ratio enhances the depletion attraction. The volume fraction, $\phi$, occupied by the spheroids is related to the bulk number density, $\rho_{\mathrm{b}}$, as

$$\phi_{\mathrm{Prolate}} = \frac{4}{3}\pi\alpha\beta^2\rho_{\mathrm{b}} \quad [26a]$$

$$\phi_{\mathrm{Oblate}} = \frac{4}{3}\pi\alpha^2\beta\rho_{\mathrm{b}}. \quad [26b]$$

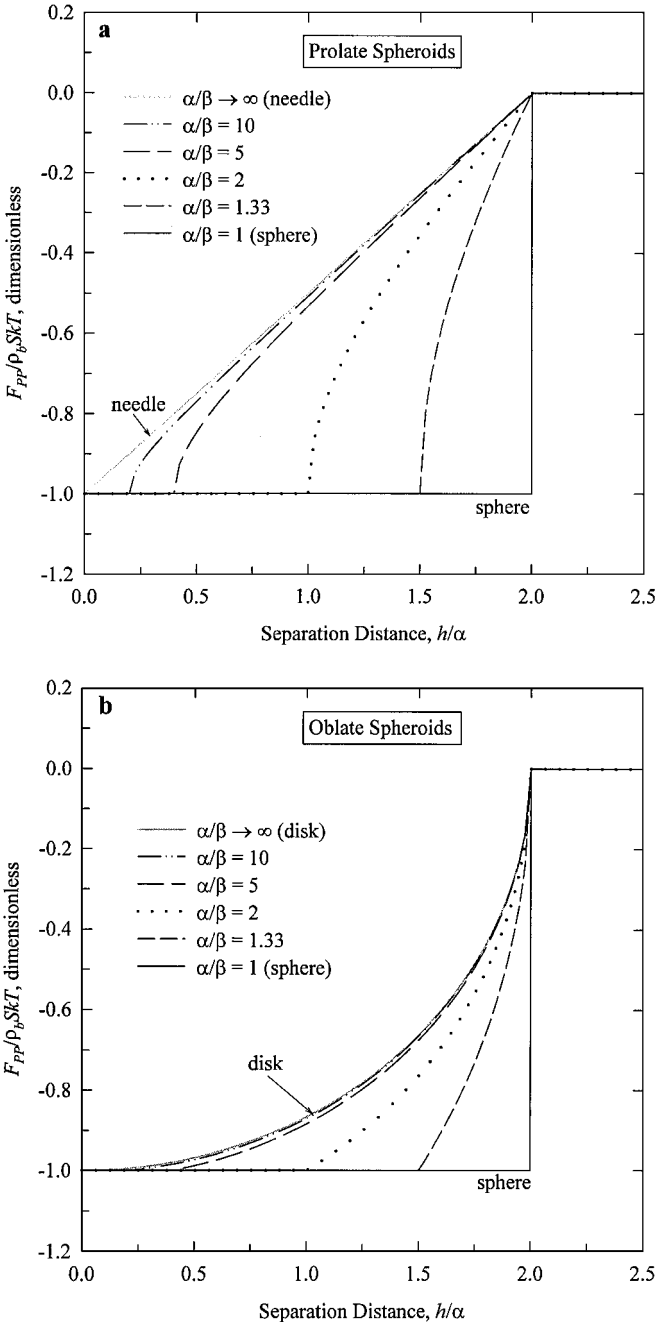


**FIG. 3.** The effect of macromolecule shape on the depletion force between two parallel plates in an uncharged, hard system of prolate (a) and oblate (b) spheroids. Here, the dimensionless depletion force is plotted as a function of the dimensionless gap width. The different curves shown correspond to various aspect ratios, $\alpha/\beta$, of the spheroids. The results for spherical ($\alpha/\beta = 1$), needle-like, and disk-like ($\alpha/\beta \to \infty$) macromolecules are presented for comparison.

By comparison, in Fig. 6 the macromolecule volume fraction stays fixed with varying aspect ratio. Now the number density changes and *increasing* the spheroid aspect ratio significantly enhances the depletion effect. Similar to the case of the spheroidal macromolecules between two plates, the force and energy produced by oblate spheroids (Figs. 5b and 6b) are significantly

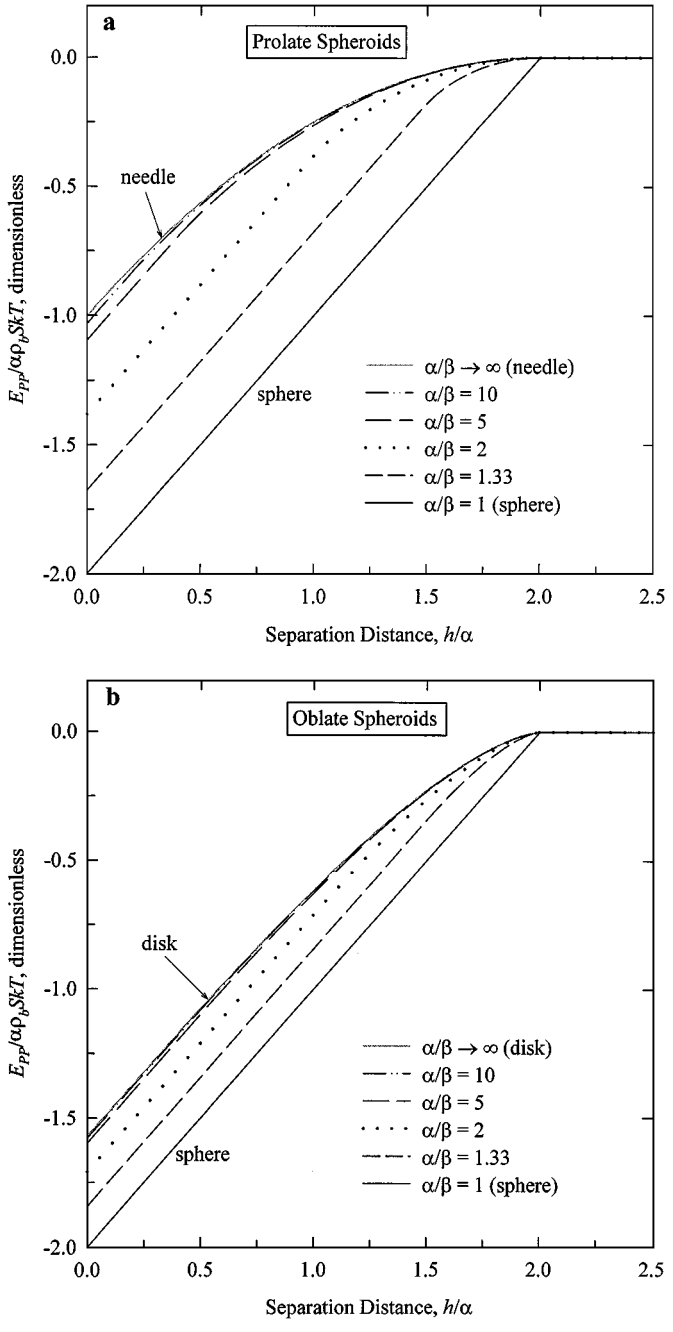


**FIG. 4.** The effect of macromolecule shape on the depletion energy between two parallel plates in an uncharged, hard system of prolate (a) and oblate (b) spheroids. Here, the dimensionless depletion energy is plotted as a function of the dimensionless gap width. The different curves shown correspond to various aspect ratios, $\alpha/\beta$, of the spheroids. The results for spherical ($\alpha/\beta = 1$), needle-like, and disk-like ($\alpha/\beta \to \infty$) macromolecules are presented for comparison.

closer to those for spherical macromolecules than the force and energy produced by prolate spheroids (Figs. 5a and 6a). The spherical macromolecule results shown in Figs. 5 and 6 were computed using Eq. [25]. A summary of the data presented in Figs. 5 and 6 is given in Table 1.

*Particle–Macromolecule Interactions in Charged Systems*

When the particles and macromolecules possess a net charge, the particle–macromolecule interaction energy becomes a continuous function of the relative orientation angle, $\theta$. Figure 7a

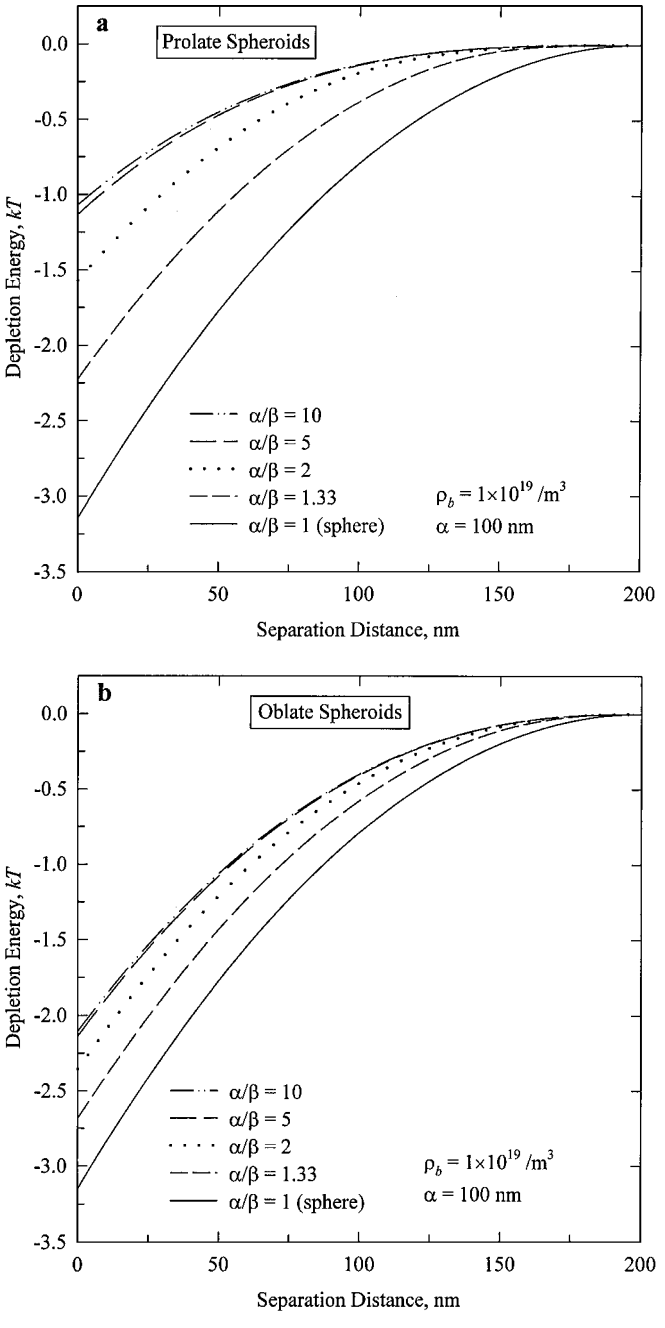


**FIG. 5.** The effect of macromolecule shape on the depletion interaction between two 5-$\mu$m-radius spherical particles in a solution of prolate (a) and oblate (b) spheroids. The macromolecules and particles are treated as hard spheroids (100 nm semimajor axis length, $\alpha$) and hard spheres, respectively. The macromolecule number density ($\rho_b = 1.0 \times 10^{19}$ macromolecules/m$^3$) remains fixed and the volume fraction is allowed to vary with varying aspect ratio, $\alpha/\beta$. In both cases, the results for spherical macromolecules ($\alpha/\beta = 1$) are presented for comparison.

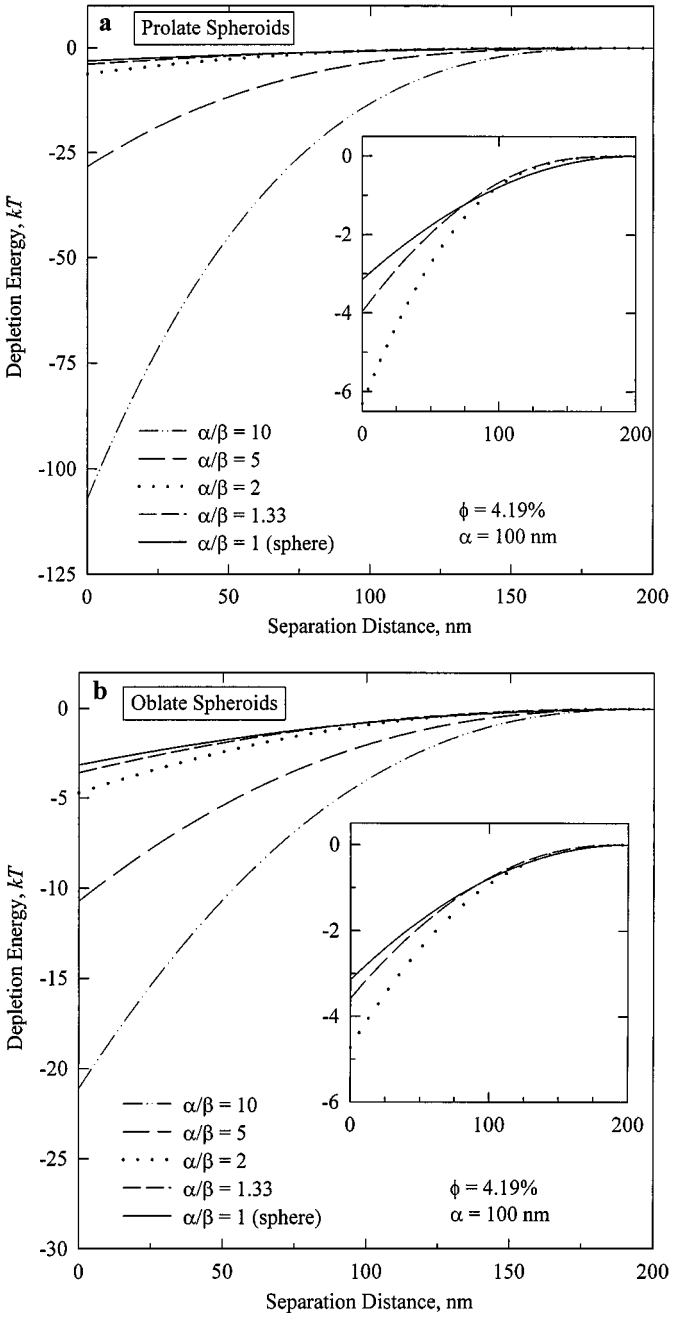


**FIG. 6.** The effect of macromolecule shape on the depletion interaction between two 5-$\mu$m-radius spherical particles in a solution of prolate (a) and oblate (b) spheroids. The macromolecules and particles are treated as hard spheroids (100-nm semimajor axis length, $\alpha$) and hard spheres, respectively. The macromolecule volume fraction ($\phi = 4.19\%$) remains fixed and the number density is allowed to vary with varying aspect ratio, $\alpha/\beta$. In both cases, the results for spherical macromolecules ($\alpha/\beta = 1$) are presented for comparison. The inserts in (a) and (b) show an expanded view for low aspect ratio spheroids.

illustrates this interaction for prolate spheroids of varying aspect ratio. The particle here is treated as a hard, charged sphere with radius $R = 5\ \mu$m, while the macromolecule is modeled as a nonadsorbing, hard, charged spheroid with the semimajor axis length equal to 100 nm. Both surfaces are assumed to have constant surface potentials of $-50$ mV, while the solution Debye length, $\kappa^{-1}$, is kept at 10 nm (approximately equal to 1 mM of monovalent electrolyte). Equations [8]–[13] were used to calculate the interaction energy as a function of the spheroid orientation angle $\theta$ at a fixed particle–macromolecule center–center distance of 5.12 $\mu$m. Because of the symmetry of the sphere–spheroid system, the orientation can be described with only one angle and only the results for $\theta$ between 0 and $\pi/2$ need to be computed. At a given particle–macromolecule separation, the interaction energy reaches a maximum for $\theta = 0$ and decreases very rapidly with increasing $\theta$. Moreover, the energy is higher and decreases less rapidly for lower aspect ratio spheroids.

At low macromolecule concentrations, the probability of finding a macromolecule at position $\mathbf{x}$ and orientation $\mathbf{\Omega}$ will be given by a Boltzmann distribution function. Thus

$$P(x, \theta) \sim \exp\left[\frac{-E(x, \theta)}{\mathrm{kT}}\right], \qquad [27]$$

where $P(x, \theta)$ is the probability, $x$ is the particle–macromolecule center-to-center distance, and $E(x, \theta)$ is the interaction energy. In Fig. 7b, the function $\exp[-E(x, \theta)/\mathrm{kT}]$ is plotted against $\theta$ for the system described above (Fig. 7a). As seen, the probability increases rapidly with increasing value of $\theta$ ($x$ is fixed at 5.12 $\mu$m here). It is essentially zero near $\theta = 0$ and approaches a maximum at around $\theta = \pi/4$ in the case of thin prolate spheroids. For thicker macromolecules (lower aspect ratios), this probability increases slower with increasing $\theta$ (i.e., for a sphere the probability would be independent of $\theta$). Whenever $x < 5.1\ \mu$m, the spheroid

**TABLE 1**
**Summary of the Results of Figs. 5 and 6 for Uncharged Systems**

| | $\alpha/\beta$ | $\rho_b$ (No./m$^3$) | $\phi$ (% vol) | $E_{dep}(0)$ (kT) |
|---|---|---|---|---|
| Prolate | 10 | $1 \times 10^{19}$ | 0.042 | −1.07 |
| spheroids | 5 | $1 \times 10^{19}$ | 0.17 | −1.13 |
| | 2 | $1 \times 10^{19}$ | 1.05 | −1.57 |
| | 1.33 | $1 \times 10^{19}$ | 2.36 | −2.22 |
| | 10 | $1 \times 10^{21}$ | 4.19 | −106.76 |
| | 5 | $2.50 \times 10^{20}$ | 4.19 | −28.26 |
| | 2 | $4.00 \times 10^{19}$ | 4.19 | −6.28 |
| | 1.33 | $1.78 \times 10^{19}$ | 4.19 | −3.95 |
| Oblate | 10 | $1 \times 10^{19}$ | 0.42 | −2.11 |
| spheroids | 5 | $1 \times 10^{19}$ | 0.84 | −2.14 |
| | 2 | $1 \times 10^{19}$ | 2.10 | −2.36 |
| | 1.33 | $1 \times 10^{19}$ | 3.14 | −2.68 |
| | 10 | $1.00 \times 10^{20}$ | 4.19 | −21.04 |
| | 5 | $5.00 \times 10^{19}$ | 4.19 | −10.68 |
| | 2 | $2.00 \times 10^{19}$ | 4.19 | −4.71 |
| | 1.33 | $1.33 \times 10^{19}$ | 4.19 | −3.58 |
| Spheres | 1 | $1 \times 10^{19}$ | 4.19 | −3.14 |

*Note.* Shown at each value of $\alpha/\beta$ is the macromolecule number density, $\rho_b$; the corresponding volume fraction, $\phi$; and the depletion energy at contact ($h = 0$).

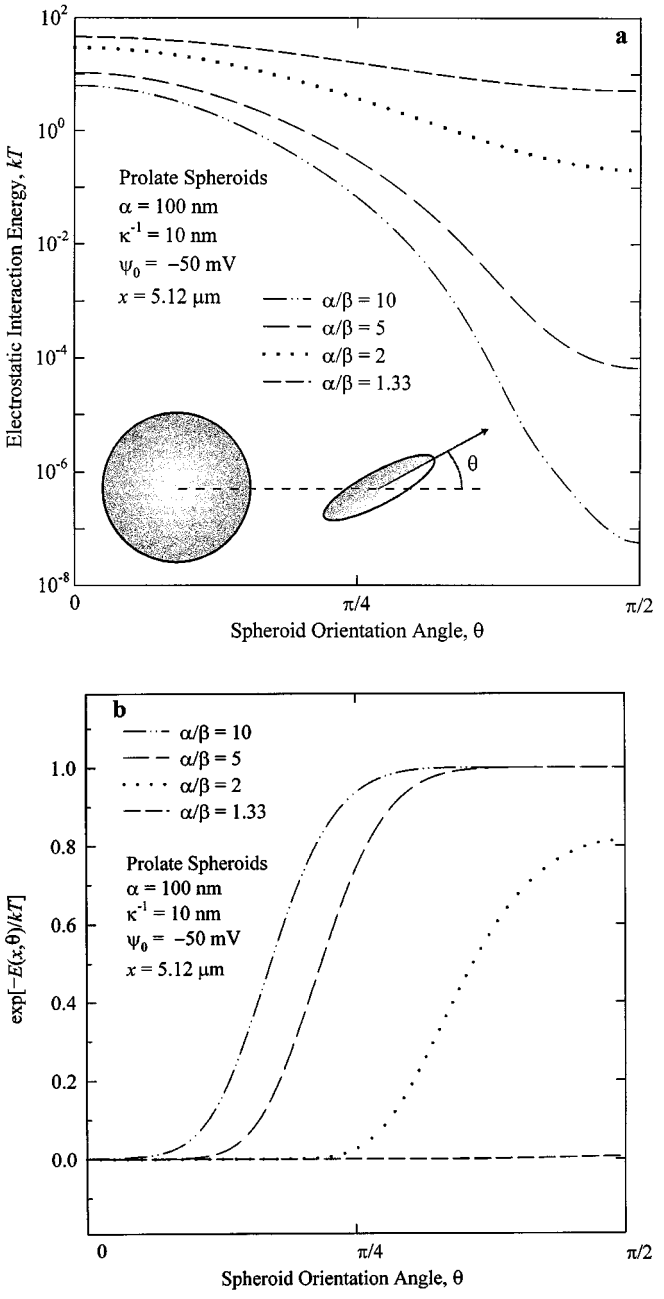


**FIG. 7.** (a) The effect of orientation on the electrostatic interaction between a 5-$\mu$m-radius spherical particle and a prolate spheroid. This energy profile is computed at a fixed center–center separation $x = 5.12$ $\mu$m for the range of spheroid orientations $0 < \theta < \pi/2$. Both surfaces are assumed to have $-50$ mV surface potentials and the solution Debye length is 10 nm. The length of the semimajor axis, $\alpha$, is 100 nm in all cases. (b) The function $\exp[-E(x, \theta)/\mathrm{kT}]$, which is proportional to the probability of finding a macromolecule at $x$ in orientation $\theta$.

touches or penetrates the particle in the range $0 < \theta < \theta_{\text{touch}}$, where $\theta_{\text{touch}}$ is a function of the spheroid aspect ratio and $x$. In this case, the shape of the electrostatic energy profile and the corresponding probability distribution resemble those presented above in the range $\theta_{\text{touch}} < \theta < \pi/2$. Finally, for a fixed value of $\theta$, the electrostatic energy decreases with increasing $x$ and consequently the probability of finding a macromolecule is greater at larger separations.

### *Depletion Interactions in Charged Spheroid Systems*

The effect of macromolecule shape on the depletion interaction between two negatively charged, 5-$\mu$m-radius particles immersed in a solution of charged, spheroidal macromolecules (100 nm semimajor axis length) is presented in Fig. 8. The particles are treated as hard, charged spheres, while the macromolecules are modeled as nonadsorbing, hard, charged prolate spheroids. All surfaces are assumed to have constant surface potentials of $-50$ mV and the solution Debye length is 10 nm. The depletion force is computed using the modified force balance model (Eq. [5]) with the expressions for particle–macromolecule interactions determined from Eqs. [8]–[13]. In the case of a constant macromolecule number density (Fig. 8a), *decreasing* the spheroid aspect ratio enhances the depletion attraction. At constant volume fraction (Fig. 8b), on the other hand, *increasing* the spheroid aspect ratio significantly enhances the interaction. Table 2 summarizes the data presented in Figs. 8a and 8b. Although the same trends are observed in the uncharged system, the depletion effect is considerably larger and longer ranged in the charged system.

Due to limitations of the model describing an electrostatic potential distribution around a spheroid (Eqs. [11]–[12]), the depletion interactions in charged systems were determined for prolate macromolecules only. This subject is discussed further below.

## DISCUSSION

### *Interactions in Noncharged Systems*

*Scaling relationships.* In attempting to understand the major trends in Figs. 3–6, it will be helpful to develop some

**TABLE 2**
**Summary of the Results of Fig. 8 for Charged Systems**

| | $\alpha/\beta$ | $\rho_b$ (No./m$^3$) | $\phi$ (% vol) | $E_{dep}(0)$ (kT) |
|---|---|---|---|---|
| Prolate | 10 | $1 \times 10^{19}$ | 0.042 | −2.58 |
| spheroids | 5 | $1 \times 10^{19}$ | 0.17 | −3.27 |
| | 2 | $1 \times 10^{19}$ | 1.05 | −5.37 |
| | 1.33 | $1 \times 10^{19}$ | 2.36 | −7.18 |
| | 10 | $1.00 \times 10^{21}$ | 4.19 | −258.40 |
| | 5 | $2.50 \times 10^{20}$ | 4.19 | −81.80 |
| | 2 | $4.00 \times 10^{19}$ | 4.19 | −21.49 |
| | 1.33 | $1.78 \times 10^{19}$ | 4.19 | −12.77 |
| Spheres | 1 | $1 \times 10^{19}$ | 4.19 | −8.96 |

*Note.* Shown at each value of $\alpha/\beta$ is the macromolecule number density, $\rho_b$; the corresponding volume fraction, $\phi$; and the depletion energy at contact ($h = 0$).

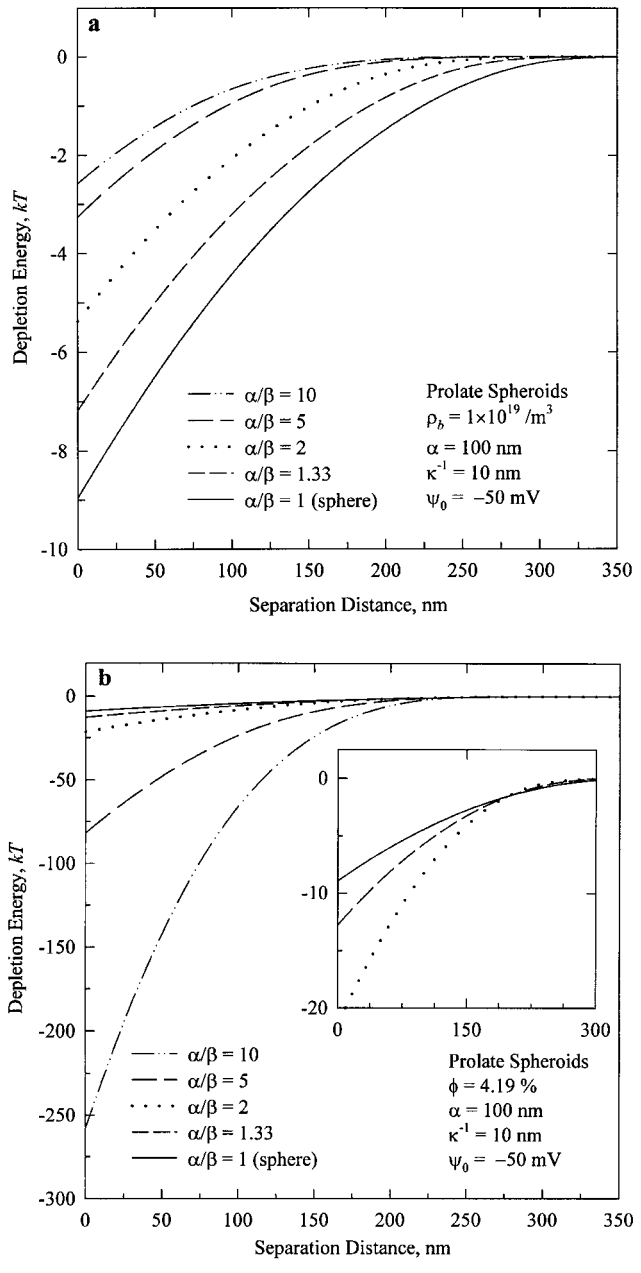


**FIG. 8.** The effect of macromolecule shape on the depletion interaction between two 5-$\mu$m-radius spherical particles. All surfaces are assumed to have $-50$-mV surface potentials with solution Debye length equal to 10 nm. The macromolecules are modeled as prolate spheroids (semimajor axis length, $\alpha$, equal to 100 nm) with varying aspect ratio, $\alpha/\beta$. (a) The effect when the macromolecule number density, $\rho_b$, remains fixed at $1 \times 10^{19}$ macromolecules/m$^3$. (b) The effect for a constant volume fraction, $\phi$, equal to 4.19%. In both cases, the results for spherical macromolecules ($\alpha/\beta = 1$) are presented for comparison. The insert in (b) shows an expanded view for low aspect ratio spheroids.

simple scaling relationships describing the dependence of the interaction energy at contact ($h = 0$), on the macromolecule shape, size, and concentration (the attraction is maximum at contact.) For the parallel plate geometry, Eqs. [20a] and [20b] simplify to

$$\frac{E_{\mathrm{PP,Prolate}}(h=0)}{\rho_b \mathrm{SkT}\alpha} = -1 - \frac{\ln(A+\sqrt{A^2-1})}{A\sqrt{A^2-1}} \quad [28a]$$

$$\frac{E_{\mathrm{PP,Oblate}}(h=0)}{\rho_b \mathrm{SkT}\alpha} = -\frac{1}{A} + \frac{A}{\sqrt{A^2-1}}\left[\tan^{-1}\left(\frac{1}{\sqrt{A^2-1}}\right) - \frac{\pi}{2}\right] \quad [28b]$$

and reduce further in the case of spherical macromolecules ($A = 1$) to

$$\frac{E_{\mathrm{PP,Sphere}}(h=0)}{\rho_b \mathrm{SkT}a} = -2, \quad [29]$$

where $a$ here denotes the macromolecule radius. Thus the ratio of the contact energy due to spheroidal macromolecules to that caused by spherical macromolecules will be given by

$$\frac{E_{\mathrm{PP,Prolate}}(h=0)}{E_{\mathrm{PP,Sphere}}(h=0)} = \frac{1}{2} + \frac{\ln(A+\sqrt{A^2-1})}{2A\sqrt{A^2-1}} \quad \text{constant } \rho_b \quad [30a]$$

$$\frac{E_{\mathrm{PP,Oblate}}(h=0)}{E_{\mathrm{PP,Sphere}}(h=0)} = \frac{1}{2A} - \frac{A}{2\sqrt{A^2-1}}\left[\tan^{-1}\left(\frac{1}{\sqrt{A^2-1}}\right) - \frac{\pi}{2}\right] \quad \text{constant } \rho_b \quad [30b]$$

in the case of prolate and oblate macromolecules, respectively.

Similarly for the geometry of two large spherical particles, the interaction energy at contact can be obtained from Eqs. [21a] and [21b] as

$$\frac{E_{\mathrm{SS,Prolate}}(h=0)}{\mathrm{kT}} = -\rho_b \pi R\alpha^2\left(\frac{2}{3} + \frac{4}{3}A^{-2}\right) = -\phi R\alpha^{-1}\left(\frac{A^2}{2} + 1\right) \quad \text{for } R \gg \alpha \quad [31a]$$

$$\frac{E_{\mathrm{SS,Oblate}}(h=0)}{\mathrm{kT}} = -\rho_b \pi R\alpha^2\left(\frac{4}{3} + \frac{2}{3}A^{-2}\right) = -\phi R\alpha^{-1}\left(A + \frac{1}{2}A^{-1}\right) \quad \text{for } R \gg \alpha \quad [31b]$$

for prolate and oblate macromolecules, respectively. These equations can be used to understand the dependence of the energy on the size and shape of the spheroidal macromolecules. Specifically, for a given $\alpha$ value, the magnitude of the depletion

interaction decreases with increasing aspect ratio for constant $\rho_b$ and increases with increasing aspect ratio for constant $\phi$.

The magnitude of these interactions relative to the case of spherical macromolecules can be determined by letting the aspect ratio go to 1.0,

$$\frac{E_{SS,Sphere}(h=0)}{kT} = -2\rho_b \pi R a^2 = -\frac{3}{2}\phi R a^{-1} \quad \text{for } R \gg a, \quad [32]$$

where $a$ denotes the macromolecule radius. The ratio of the contact energy due to spheroidal macromolecules to that caused by spherical macromolecules for the conditions of equal macromolecule number densities and equal macromolecule volume fractions are given by the following relationships:

$$\frac{E_{SS,Prolate}(h=0)}{E_{SS,Sphere}(h=0)} = \frac{1}{3}\left(1+\frac{2}{A^2}\right) \quad \text{for } R \gg \alpha \text{ and constant } \rho_b \quad [33a]$$

$$\frac{E_{SS,Prolate}(h=0)}{E_{SS,Sphere}(h=0)} = \frac{1}{3}(2+A^2) \quad \text{for } R \gg \alpha \text{ and constant } \phi \quad [33b]$$

$$\frac{E_{SS,Oblate}(h=0)}{E_{SS,Sphere}(h=0)} = \frac{1}{3}\left(2+\frac{1}{A^2}\right) \quad \text{for } R \gg \alpha \text{ and constant } \rho_b \quad [33c]$$

$$\frac{E_{SS,Oblate}(h=0)}{E_{SS,Sphere}(h=0)} = \frac{1}{3}\left(2A+\frac{1}{A}\right) \quad \text{for } R \gg \alpha \text{ and constant } \phi. \quad [33d]$$

In the $A \to \infty$ limit, these equations simplify to

$$\frac{E_{SS,Needle}(h=0)}{E_{SS,Sphere}(h=0)} = \frac{1}{3} \quad \text{for } R \gg \alpha \text{ and constant } \rho_b \quad [34a]$$

$$\frac{E_{SS,Needle}(h=0)}{E_{SS,Sphere}(h=0)} = \frac{A^2}{3} \quad \text{for } R \gg \alpha \text{ and constant } \phi \quad [34b]$$

$$\frac{E_{SS,Disk}(h=0)}{E_{SS,Sphere}(h=0)} = \frac{2}{3} \quad \text{for } R \gg \alpha \text{ and constant } \rho_b \quad [34c]$$

$$\frac{E_{SS,Disk}(h=0)}{E_{SS,Sphere}(h=0)} = \frac{2A}{3} \quad \text{for } R \gg \alpha \text{ and constant } \phi \quad [34d]$$

for needle-like and disk-like macromolecules, respectively. Equations [33a]–[33d] can be used to further understand the results summarized in Table 1. Because $A \geq 1$, the depletion attraction due to spheroids will always be smaller than the attraction caused by spheres at equal macromolecule number densities. However, at equal macromolecule volume fractions, the opposite will be true (i.e., the depletion attraction due to spheroids will be larger than that produced by spheres). This latter trend was reported previously for the case of rod-like macromolecules (34, 45, 52).

These trends can be understood physically by recognizing that the attraction arises because the macromolecules are excluded from the gap region at sufficiently small gaps. As the aspect ratio increases, meaning that the macromolecules become more needle-like or disk-like, the number of allowable orientations in the gap increases. Thus for a fixed number density of macromolecules, the interaction decreases because the thinner spheroids can more easily access the gap region. When the volume fraction is held constant, however, the dominant effect is the higher number density of spheroids needed to maintain a given volume fraction at increasing aspect ratios. Thus the interaction actually increases.

It is also instructive to compare $E_{Dep}(h=0)$ for prolate and oblate spheroids having the same aspect ratio. Dividing Eq. [33a] by [33c] and Eq. [33b] by [33d] yields the following expressions:

$$\frac{E_{SS,Prolate}(h=0)}{E_{SS,Oblate}(h=0)} = \frac{2+A^2}{1+2A^2} \quad \text{for } R \gg \alpha \text{ and constant } \rho_b \quad [35a]$$

$$\frac{E_{SS,Prolate}(h=0)}{E_{SS,Oblate}(h=0)} = \frac{2A+A^3}{1+2A^2} \quad \text{for } R \gg \alpha \text{ and constant } \phi. \quad [35b]$$

Again, since $A \geq 1$, the energy produced by oblate spheroids will always be larger than the energy produced by prolate spheroids at equal aspect ratios and number densities. Conversely, at equal $\phi$, the energy due to oblates will be smaller than the energy due to prolates. Along with the analysis carried out earlier (Eqs. [33a]–[33d]), these results indicate that when the length of the spheroid semimajor axis is equal to the sphere radius, the force and energy produced by oblate spheroids will be significantly closer to those for spherical macromolecules than the force and energy produced by prolate spheroids. This is because for given semimajor and semiminor axis lengths, the volume of an oblate spheroid is larger than the volume of a prolate spheroid ($V_{Prolate} = \frac{4}{3}\pi\alpha\beta^2$ and $V_{Oblate} = \frac{4}{3}\pi\alpha^2\beta$), meaning that the oblate spheroid has fewer allowable orientations in the gap region between two particles.

*Validity of Derjaguin approximation.* Because the Derjaguin approximation was used to derive the analytical expressions describing the depletion interactions in noncharged systems (Eqs. [21]–[24]), it is useful to consider its limitations. Based on the assumption that the particle radius is much larger than the range of the interaction, this approximation is expected to become less accurate for smaller values of $R/L$ (the ratio of the particle radius to the largest macromolecule dimension,

represented by $L$). In addition, the magnitude of the percentage error, defined as

$$\%\text{error} = \frac{|E_{\text{Rigorous}} - E_{\text{Derjaguin}}|}{E_{\text{Rigorous}}} \times 100, \qquad [36]$$

is expected to increase with gap width, since the Derjaguin approximation also assumes that $h \ll R$ (i.e., curvature effects are insignificant). For simplicity, only the error at contact ($h = 0$) will be considered.

In the case of spherical macromolecules, Eqs. [24] and [25] give appropriate expressions for $E_{\text{Derjaguin}}$ and $E_{\text{Rigorous}}$, respectively. The Derjaguin approximation is found to underestimate the depletion interaction (i.e., $E_{\text{Derjaguin}} < E_{\text{Rigorous}}$) with an error at contact less than 1% whenever $R/a > 70$ ($a$ here refers to the radius of the spherical macromolecule). This deviation increases steadily with decreasing $R/a$ ratio, becoming 15% at $R/a = 4$, for example. This error arises from the fact that as the ratio $R/a$ decreases, the region of the spherical particles surface comprising the exclusion zone increases, and the parabolic function used to describe the spherical surface in the Derjaguin approximation becomes a poorer representation of the interaction region.

A similar analysis can be performed for spheroidal macromolecules by comparing the predictions of Eqs. [21a] and [21b] (approximate expressions describing the depletion attraction in the Derjaguin limit) to the rigorous results computed with the force balance model (Eqs. [5]–[7]). It is found that the approximate model underestimates the depletion interaction for oblate macromolecules, but overestimates the interaction for prolate macromolecules. This latter result was reported earlier by Yaman *et al.* (53) for the case of thin rod-like macromolecules ($L/D \gg 1$, where $D$ represents the rod diameter). For example, in the case of prolate macromolecules with $R/\alpha = 4$ and aspect ratio equal to 5, the error is approximately 25% at contact, and is only slightly larger (approximately 32% error) at infinite aspect ratio.

### *Interactions in Charged Systems*

*Validity of the electrostatic model.* The validity of the linear superposition approximation has already been discussed in the Theory section. The potential distributions around the spherical macromolecules and particles were calculated using Eq. [10], which requires $\kappa R \geq 10$ and surface potentials $\leq$200 mV. Each of these requirements was satisfied in the calculations presented here for both the particles and macromolecules. The only remaining issue is then the validity of the perturbation solution for describing the electric potential around the spheroidal macromolecules.

As mentioned earlier, the perturbation method is most accurate for double layers that are much smaller than the macromolecule size. It can be also applied to moderate or even thick double layers as long as the spheroid aspect ratio stays sufficiently large. For example, the model would not apply to thin prolate shapes or spheres with radius comparable to $\kappa^{-1}$. From the data in Tables 1 and 2 of the Hsu and Liu paper (55), it can be deduced that the average error in the perturbation treatment for the case of a prolate spheroid having $\alpha/\beta = 1.67$ and $\kappa\alpha = 10$ is on the order of 6%. Furthermore, this deviation is largest in the regions of highest curvature (i.e., spheroid poles in the case of prolate macromolecules), approaching 10% in these regions, and lowest where the curvature is minimum (approximately 2%). As seen in Fig. 7b, the probability of the spheroid having an orientation angle of $\pi/2$ (semimajor axis parallel to sphere tangent) is much greater than the probability of a $\theta = 0$ orientation (pole of spheroid toward sphere). This suggests that the 2% error reported by Hsu and Liu may be a better characterization of the error in the spherical particle/spheroidal macromolecule interaction energy for these particular values of $\alpha$ and $\beta$.

The results presented here for the depletion interaction in charged systems are thus believed to be within a few percent of the true value when the spheroid aspect ratio is less than two. This error increases with increasing aspect ratio, and the error in systems where $\alpha/\beta$ is greater than 10 is difficult to quantify. As shown in Fig. 7b, however, as the aspect ratio increases, the probability of the spheroid having an orientation parallel to the sphere's tangent, where the perturbation model is most accurate, also increases. Thus the model may be reasonably accurate even at these large aspect ratios. Testing this accuracy would require more rigorous models describing the electrostatic potential around the spheroids.

*Magnitude of the effect of charge on the depletion interactions.* The magnitude of the depletion interaction in charged and noncharged systems follows the same trends with macromolecule size and shape as seen in the unchanged systems. In particular, for a constant macromolecule number density, decreasing the spheroid aspect ratio enhances the depletion attraction, while at constant volume fraction, the opposite is true.

The effect of charge on the depletion attraction can be understood by introducing an "effective" macromolecule size, reflecting both the size of the hard core of the macromolecule and the thickness of the surrounding ion cloud, which will be on the order of the solution Debye length. Although the effect of charge can be significantly more complex, this approach nonetheless provides a tool for understanding the qualitative trends in the results.

If the extra size produced by the ion cloud is denoted as $\delta$, then the attractive energy at contact for two large spherical particles in solution with prolate and oblate macromolecules becomes

$$\frac{E_{\text{SS,Prolate,Charged}}(h=0)}{R\,\text{kT}} = -\rho_b \pi(\alpha+\delta)^2\left[\frac{2}{3} + \frac{4}{3}(A')^{-2}\right] = -\phi\frac{(\alpha+\delta)^2}{\alpha^3}A^2\left[\frac{1}{2} + (A')^{-2}\right] \qquad \text{for } R \gg \alpha \quad [37a]$$

$$\frac{E_{\mathrm{SS,Oblate,Charged}}(h=0)}{R\,\mathrm{kT}}$$
$$= -\rho_{\mathrm{b}}\pi(\alpha+\delta)^2\left[\frac{4}{3}+\frac{2}{3}(A')^{-2}\right]$$
$$= -\phi\frac{(\alpha+\delta)^2}{\alpha^3}A\left[1+\frac{1}{2}(A')^{-2}\right] \qquad \text{for } R \gg \alpha, \quad [37b]$$

where

$$A = \frac{\alpha}{\beta} \quad \text{and} \quad A' = \frac{(\alpha+\delta)}{(\beta+\delta)}. \qquad [37c]$$

In the case of spherical macromolecules ($A = 1$) these equations simplify to

$$\frac{E_{\mathrm{SS,Sphere,Charged}}(h=0)}{R\,\mathrm{kT}} = -2\rho_{\mathrm{b}}\,\pi(a+\delta)^2 = -\frac{3}{2}\phi\frac{(a+\delta)^2}{a^3} \qquad \text{for } R \gg a, \quad [38]$$

where $a$ denotes the macromolecule radius. It should be noted that the effect of the ion cloud on the effective radius of the particle is being ignored, which is strictly correct only when $\kappa R \gg 1$.

As the thickness of the double layer increases (i.e., increasing $\delta$), $A'$ decreases, approaching a lower limit of 1.0 as $\delta \to \infty$. Thus according to Eq. [37], adding charge increases the magnitude of the depletion attraction for both the constant $\rho_{\mathrm{b}}$ and constant $\phi$ cases for all macromolecule shapes. The effect is much more pronounced when the characteristic size of the macromolecules is smaller than the Debye length. In addition, for the case where the Debye length is much greater than either the semimajor or semiminor axes, $A' \approx 1$ and the interactions for both the prolate and oblate shapes become equal to that of equivalently sized spheres.

For example, for a system containing 5-$\mu$m-radius particles and prolate macromolecules with $\alpha = 100$ nm and $A = 5$ at constant macromolecule number density, adding $-50$-mV potentials to the particles and macromolecules in a solution where $\kappa^{-1} = 10$ nm increases the magnitude of the interaction at contact by a factor of 2.9 relative to the case of uncharged particles and macromolecules. (The interaction for the charged system was calculated using the rigorous force-balance model.) Matching this increase using the simplified approach of Eq. [37] requires an effective double-layer thickness, $\delta$, of approximately 5 Debye lengths.

Note that the approach described here for approximating the effect of charge in spheroidal macromolecule systems assumes that the effective thickness of the double-layer is uniform on all parts of the spheroid surface. In a recent paper, Piech and Walz (60) showed that using two different effective thicknesses (i.e., one for the semimajor axis and one for the semiminor axis) does not lead to a significant improvement in the accuracy of the approximation.

*Interactions between Macromolecules*

In using the Boltzmann equation to calculate the density distribution of macromolecules around the spherical particles (Eq. [2]), interactions between the macromolecules themselves were ignored. Such interactions have been shown to produce structuring of the macromolecules and oscillations in the resulting depletion force profile between two macroscopic surfaces (32, 36, 39–43, 45). The accuracy of the results presented above depends upon the validity of this assumption of ideal behavior.

In uncharged systems of hard spherical macromolecules, Walz and Sharma showed that higher order concentration effects will be negligible for volume concentrations up to about 1% (42). As seen in Tables 1 and 2, however, the first-order model (Eqs. [4] and [25]) was used to predict depletion interactions in solutions of spherical macromolecules at volume fractions as large as 4.19%. Although this results in some error, the magnitude of structural repulsion predicted with the second-order force balance model of Walz and Sharma (42) at this volume fraction did not exceed 1 kT, while the depletion attraction was not significantly affected. For example, in the hard sphere system at $\phi = 4.19\%$, the energy at contact calculated with the first-order treatment differed by less than 1% from the second-order model predictions. In addition, the barrier height computed with the second-order model was only 0.12 kT.

Mao *et al.* showed that for thin noncharged rod-like macromolecules and reduced number densities of order unity ($c_{\mathrm{b}} \equiv \rho_{\mathrm{b}} DL^2 \sim 1$, where $c_{\mathrm{b}}$ denotes the reduced density, while $D$ and $L$ are the rod diameter and length, respectively), the repulsive barrier is typically much smaller than the thermal energy kT (40). The authors attributed this lower-than-expected barrier to offsetting second- and third-order effects. As illustrated in Fig. 4a, the potential profile for prolate spheroids with aspect ratios greater than 10 is very similar to that of rods. For the cases considered here in which the aspect ratio was 10, the reduced density ($c_{\mathrm{b}} \equiv \rho_{\mathrm{b}}(2\beta)(2\alpha)^2$) never exceeded 0.8, suggesting that the finding of Mao *et al.* would apply here.

In summary, based on the results of Walz and Sharma for spherical macromolecules (low aspect ratio) and Mao *et al.* for rods (high aspect ratio), we conclude that higher order effects would not significantly alter the results presented here, especially in noncharged systems. In the charged systems higher order effects will clearly be more important, as the effective volume fraction of the macromolecules will be greater. The exception would be cases in which the characteristic size of the spheroids is much larger than the Debye length, which is true for the systems studied here with $A \leq 2$.

*Effects of Depletion Interaction on the Total Interparticle Potential Energy*

Finally, it is interesting to compare the magnitude of the depletion interaction with the other interactions that can exist between particles in solution, specifically the van der Waals and electrostatic interactions. The stability of a dispersion of particles will

only be altered if the depletion interaction is significant relative to these other interactions.

The system studied is two relatively large particles interacting across a separation distance near the location of the secondary potential energy well. Specifically, the gap width, $h$, is much larger than the Debye length, $\kappa^{-1}$, yet much smaller than the particle radius, $R$. These conditions are chosen as they allow use of the linear superposition approximation to estimate the electric potential in the gap along with the Derjaguin approximation to account for the particle curvature.

Under these conditions, the van der Waals interaction energy can be calculated using the Derjaguin approach, as

$$E_{\text{vdw}}(h) = -\frac{R}{12}\int_h^\infty \frac{A(h')}{h'^2}\,\mathrm{d}h', \qquad [39]$$

where $A(h')$ is the effective Hamaker constant calculated between two infinite half-spaces separated by gap width $h'$. For these calculations, $A(h')$ was calculated using the Lifshitz equations (61). Likewise, the electrostatic interaction can be estimated as (62)

$$E_{\text{Elec.}}(h) = B\exp(-\kappa h), \qquad [40]$$

where $B$ is a function of the surface potentials (assumed $-50$ mV here) and sizes of the two spheres. For these calculations, $R$ for both polystyrene spheres was assumed to be 5 $\mu$m and the Debye length was 10 nm ($\kappa R = 500$).

The results are shown in Fig. 9. The solid line represents the interaction with no added macromolecules (i.e., sum of Eqs. [39] and [40]). For the dashed line, the depletion interaction produced by the addition of 100 nm radius spheres, also with $-50$ mV surface potentials, at a bulk volume fraction of 4.19% is included. Now, a secondary well of approximately 4 kT is produced. For the other two curves in the graph, the 100-nm-radius spheres are replaced by prolate spheroids with a major axis length of 100 nm and an aspect ratio of 5. For the broken line, the volume fraction is 4.19%, while for the dotted line the number density is the same as for the spherical macromolecule case (the volume fraction is now 0.17%). At the same volume fraction, the depth of the secondary well is increased to over 30 kT, which is easily sufficient to cause secondary flocculation. On the other hand, at a constant number density, moving from the spherical to spheroidal shape reduces the well depth from 4 to 1.3 kT, which would not have a significant effect on the stability of a dispersion of such particles. In the Derjaguin limit, the magnitude of these energy wells scales with the particle radius.

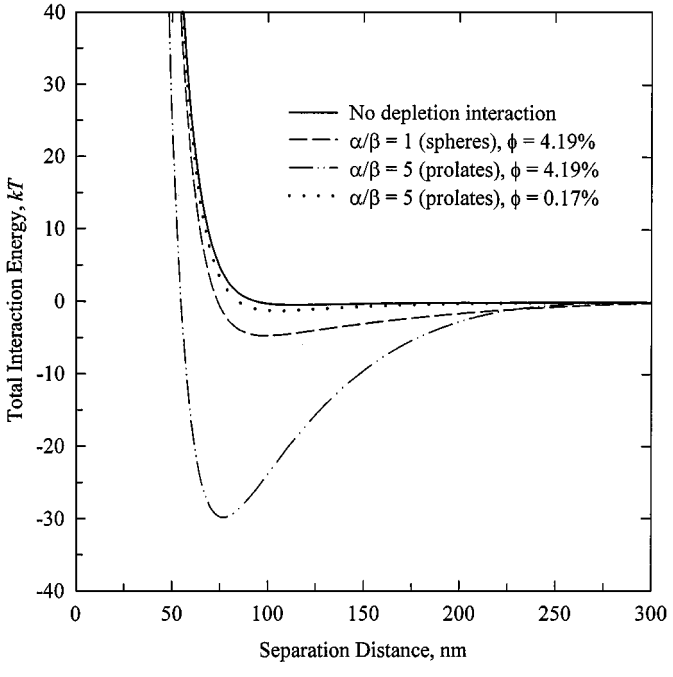


**FIG. 9.** The effect of the depletion interaction on the total energy profile between two 5-$\mu$m polystyrene spheres in an aqueous solution ($\kappa^{-1} = 10$ nm) of charged macromolecules. All surfaces are charged to $-50$ mV surface potentials. The solid line consists of the electrostatic and van der Waals interactions only, while the other lines include the depletion energy produced by spherical and spheroidal macromolecules. For the dashed and broken lines, the volume fraction is fixed at 4.19%, while for the dotted line the number density is the same as for the spherical macromolecule case (i.e., the volume fraction is now 0.17%). The radius of the spherical macromolecules and the semimajor axis of the prolate spheroidal macromolecules ($\alpha/\beta = 5$) are equal to 100 nm.

## CONCLUSIONS

The general force-balance model developed by Walz and Sharma (42) was modified to calculate the interaction force and energy between two spherical particles in solution with nonadsorbing spheroidal macromolecules of arbitrary size and aspect ratio. Both purely hard wall interactions and longer-range electrostatic interactions between the particles and macromolecules were considered. Furthermore, it was assumed that the density of macromolecules was low enough that higher order effects arising from interactions between macromolecules were negligible. Analytical expressions describing the depletion interaction between hard, uncharged plates and hard, uncharged spherical particles in the $R/L \ll 1$ limit ($L$ represents the largest macromolecule dimension and $R$ is the particle radius) were also presented.

It was found that the macromolecule shape significantly affects the depletion interaction. Specifically, when the number density of macromolecules is held constant, the depletion attraction is found to decrease with increasing aspect ratio of the spheroidal macromolecules. Conversely, under the condition of constant volume fraction, the attraction increases with increasing aspect ratio. In this latter case (constant $\phi$), the interaction produced by prolate macromolecules is greater than that produced by oblate macromolecules of equal axes lengths. These results arise because (1) rod-like or disk-like macromolecules can more easily access the gap region between two particles than spherical macromolecules, and (2) at equal axes lengths, the volume of an oblate spheroid is larger than that of a prolate spheroid. Finally, prolate and oblate spheroids with aspect ratios

greater than 10 were found to behave like infinitely thin needles and disks, respectively.

The depletion interaction in charged systems follows the same general trends with macromolecule shape as those found in uncharged systems; however, both the range and magnitude are substantially increased. In addition, when the double-layer thickness is much greater than the lengths of the semimajor and semiminor axes of the spheroid (either prolate or oblate shapes), the depletion interaction becomes equal to that produced by equivalent spheres (i.e., sphere radius equal to the semimajor axis length).

Finally, it is found that the depletion attraction produced by charged prolate spheroids at concentrations of order 1% volume would be sufficient to induce flocculation of a dispersion of large colloidal particles (5 $\mu$m radius). Although not specifically presented here, this same behavior would also be valid for oblate spheroids, as the depletion interaction produced by oblate spheroids is larger than that produced by prolate spheroids at equal axis lengths and number densities.

## ACKNOWLEDGMENTS

Support for this work was provided by the National Science Foundation, through Grant CTS-9702773, and by the Petroleum Research Fund, administered by the American Chemical Society.

## REFERENCES

1. Sharma, A., Tan, S. N., and Walz, J. W., *J. Colloid Interface Sci.* **191,** 236 (1997).
2. Traube, I., *Gummi Ztg.* **39,** 434, 1647 (1925).
3. Bondy, C., *Trans. Faraday Soc.* **35,** 1093 (1939).
4. Li-in-on, F. K., Vincent, B., and Waite, F. A., *ACS Symp. Ser.* **9,** 165 (1975).
5. Crowell, C., Li-in-on, R., and Vincent, B., *J. Chem. Faraday Trans.* **74,** 337 (1978).
6. Sperry, P. R., Hopfenberg, H. B., and Thomas, N. L., *J. Colloid Interface Sci.* **82,** 62 (1981).
7. de Hek, H., and Vrij, A., *J. Colloid Interface Sci.* **70,** 592 (1979).
8. de Hek, H., and Vrij, A., *J. Colloid Interface Sci.* **84,** 409 (1981).
9. Clarke, J., and Vincent, B., *J. Colloid Interface Sci.* **82,** 208 (1981).
10. Gast, A. P., Hall, C. K., and Russel, W. B., *J. Colloid Interface Sci.* **96,** 251 (1983).
11. Snowden, M. J., Clegg, S. M., and Williams, P. A., *J. Chem. Soc. Faraday Trans.* **87,** 2201 (1991).
12. Snowden, M. J., Williams, P. A., Garvey, M. J., and Robb, I. D., *J. Colloid Interface Sci.* **166,** 160 (1994).
13. Seebergh, J. E., and Berg, J. C., *Langmuir* **10,** 454 (1994).
14. Ogden, A. L., and Lewis, J. A., *Langmuir* **12,** 3413 (1996).
15. Jenkins, P., and Snowden, M., *Adv. Colloid Interface Sci.* **68,** 57 (1996).
16. Liang, W., Tadros, Th. F., and Luckham, P. F., *J. Colloid Interface Sci.* **158,** 152 (1993).
17. Rawson, S., Ryan, K., and Vincent, B., *Colloids Surf.* **34,** 89 (1988).
18. Yaserbi, M., Shih, W. Y., and Aksay, I. A., *J. Colloid Interface Sci.* **142,** 357 (1991).
19. Smith, N., and Williams, P. A., *J. Chem. Soc. Faraday Trans.* **91,** 1483 (1995).
20. Sharma, A. Y., Tan, S. N., and Walz, J., *J. Colloid Interface Sci.* **190,** 392 (1997).
21. Sperry, P. R., *J. Colloid Interface Sci.* **99,** 97 (1984).
22. Poon, W. C. K., and Pusey, P. N., *in* "Observation, Predition and Simulation of Phase Transitionsin Complex Fluids" (M. Baus, L. F. Rull, and J. P. Ryckaert, Eds.), pp. 3–44. Kluwer Academic, Dordrecht, 1995.
23. Poulin, P., Frances, N., and Mondain-Monval, O., *Phys. Rev. E* **59,** 4384 (1999).
24. Adams, M., and Fraden, S., *Biophys. J.* **74,** 669 (1998).
25. Adams, M., Dogic, Z., Keller, S. L., and Fraden, S., *Nature* **393,** 349 (1998).
26. Koenderink, G. H., Vliegenthart, G. A., Kluijtmans, S. G. J. M., van Blaaderen, A, Philipse, A. P., and Lekkerkerker, H. N. W., *Langmuir* **15,** 4693 (1999).
27. Russel, W. B., Saville, D. A., and Schowalter, W. R., "Colloidal Dispersions." Cambridge Univ. Press, Cambridge, England, 1989.
28. Chu, X. L., Nikolov, A., and Wasan, D. T., *Langmuir* **10,** 4403 (1994).
29. Penders, M. H., and Vrij, A., *Prog. Colloid Polym. Sci.* **89,** 1 (1992).
30. Yaman, K., Jeng, M., Pincus, P., Jeppesen, C., and Marques, C. M., *Physica A* **247,** 159 (1997).
31. Yaman, K., Pincus, P., and Marques, C. M., *Phys. Rev. Lett.* **78,** 4514 (1997).
32. Groh, B., and Dietrich, S., *Phys. Rev. E* **59,** 4216 (1999).
33. Asakura, S., and Oosawa, F., *J. Chem. Phys.* **22,** 1255 (1954).
34. Asakura, S., and Oosawa, F., *J. Polym. Sci.* **33,** 183 (1958).
35. Feigin, R. I., and Napper, D. H., *J. Colloid Interface Sci.* **75,** 525 (1980).
36. Mao, Y., Cates, M. E., and Lekkerkerker, H. N. W., *Physica (Amsterdam)* **222A,** 10 (1995).
37. Henderson D., and Lozada-Cassou, M., *J. Colloid Interface Sci.* **114,** 180 (1985).
38. Sharma, A., and Walz, J. Y., *J. Chem. Soc. Faraday Trans.* **92**(24), 4997 (1996).
39. Götzelmann, B., Evans, R., and Dietrich, S., *Phys. Rev. E* **57,** 6785 (1998).
40. Mao, Y., Cates, M. E., and Lekkerkerker, H. N. W., *J. Chem. Phys.* **106,** 3721 (1997).
41. Sieglaff, C. L., *J. Polym. Sci.* **41,** 319 (1959).
42. Walz, J. Y., and Sharma, A., *J. Colloid Interface Sci.* **168,** 485 (1994).
43. Mao, Y., *J. Phys. II France* **5,** 1761 (1995).
44. de Gennes, P., *Adv. Colloid Interface Sci.* **27,** 189 (1987).
45. Mao, Y., Cates, M. E., and Lekkerkerker, H. N. W., *Phys. Rev. Lett.* **75,** 4548 (1995).
46. Buining, P. A., *J. Phys. Chem.* **97,** 11510 (1993) and references therein.
47. Lekkerkerker, H. N. W., Buining, P., Buitenhuis, J., Vroege, G. J., and Stroobants, A., *in* "Observation, Predition and Simulation of Phase Transitionsin Complex Fluids" (M. Baus, L. F. Rull, and J. P. Ryckaert, Eds.), Kluwer Academic, Dordrecht, 1995.
48. Fraden, S., *in* "Observation, Predition and Simulation of Phase Transitionsin Complex Fluids" (M. Baus, L. F. Rull, and J. P. Ryckaert, Eds.), pp. 133–164. Kluwer Academic, Dordrecht, 1995.
49. Henderson, J. R., *Mol. Phys.* **59,** 89 (1986).
50. Derjaguin, B., *Kolloid Z.* **69,** 155 (1934).
51. Derjaguin, B., *Trans. Faraday Soc.* **36,** 203 (1940).
52. Sear, R. P., *Phys. Rev. E* **57,** 1983 (1998).
53. Yaman, K., Jeppesen, C., and Marques, C. M., *Europhys. Lett.* **42,** 221 (1998).
54. Mao, Y., Bladon, P., Lekkerkerker, H. N. W., and Cates, M. E., *Mol. Phys.* **92,** 151 (1997).
55. Hsu, J. P., and Liu, B. T., *J. Colloid Interface Sci.* **192,** 481 (1997).
56. Hsu, J. P., and Liu, B. T., *Langmuir* **14,** 5383 (1998).
57. Walz, J. Y., *J. Colloid Interface Sci.* **178,** 505 (1996).
58. Piech, M., and Walz, J. Y., *J. Colloid Interface Sci.* **225,** 134 (2000).
59. Bell, G. M., Levine, S., and McCartney, L. N., *J. Colloid Interface Sci.* **33,** 335 (1970).
60. Piech, M., and Walz, J. Y., *Langmuir*, in press.
61. Prieve, D. C., and Russel, W. B., *J. Colloid Interface Sci.* **125,** 91 (1988).
62. Verwey, E. J., and Overbeek, J. Th. G., "Theory of the Stability of Lyophobic Colloids." Elsevier, Amsterdam, 1948.